Early life exposure to perfluorooctanesulfonate (PFOS) impacts vital biological processes in *Xenopus laevis:* Integrated morphometric and transcriptomic analyses

Tayaba Ismail [a,1], Hyun-Kyung Lee [a,1], Hongchan Lee [a], Youni Kim [a], Eunjeong Kim [a], Jun-Yeong Lee [a], Kee-Beom Kim [a], Hong-Yeoul Ryu [a], Dong-Hyung Cho [a], Taeg Kyu Kwon [b], Tae Joo Park [c], Taejoon Kwon [d], Hyun-Shik Lee [a,*]

[a] KNU LAMP Research Center, KNU, Institute of Basic Sciences, BK21 FOUR KNU Creative BioResearch Group, School of Life Sciences, College of Natural Sciences, Kyungpook National University, Daegu 41566, Republic of Korea
[b] Department of Immunology, School of Medicine, Keimyung University, Daegu 42601, Republic of Korea
[c] Department of Biological Sciences, College of Information-Bio Convergence, Ulsan National Institute of Science and Technology, Ulsan 44919, Republic of Korea
[d] Department of Biomedical Engineering, College of Information-Bio Convergence, Ulsan National Institute of Science and Technology, Ulsan 44919, Republic of Korea

ARTICLE INFO

ABSTRACT

Perfluorooctanesulfonate (PFOS) is a ubiquitous environmental pollutant associated with increasing health concerns and environmental hazards. Toxicological analyses of PFOS exposure are hampered by large inter-species variations and limited studies on the mechanistic details of PFOS-induced toxicity. We investigated the effects of PFOS exposure on *Xenopus laevis* embryos based on the reported developmental effects in zebrafish. *X. laevis* was selected to further our understanding of interspecies variation in response to PFOS, and we built upon previous studies by including transcriptomics and an assessment of ciliogenic effects. Midblastula-stage *X. laevis* embryos were exposed to PFOS using the frog embryo teratogenesis assay *Xenopus* (FETAX). Results showed teratogenic effects of PFOS in a time- and dose-dependent manner. The morphological abnormalities of skeleton deformities, a small head, and a miscoiled gut were associated with changes in gene expression evidenced by whole-mount in situ hybridization and transcriptomics. The transcriptomic profile of PFOS-exposed embryos indicated the perturbation in the expression of genes associated with cell death, and downregulation in adenosine triphosphate (ATP) biosynthesis. Moreover, we observed the effects of PFOS exposure on cilia development as a reduction in the number of multiciliated cells and changes in the directionality and velocity of the cilia-driven flow. Collectively, these data broaden the molecular understanding of PFOS-induced developmental effects, whereby ciliary dysfunction and disrupted ATP synthesis are implicated as the probable modes of action of embryotoxicity. Furthermore, our findings present a new challenge to understand the links between PFOS-induced developmental toxicity and vital biological processes.

1. Introduction

Perfluorooctanesulfonate (PFOS) belongs to a class of perfluoroalkyl substances (PFAS) frequently used in consumer products and is also the most frequently detected in the environment as the end-product of the breakdown of other PFAS (Ma et al., 2023). PFOS is found worldwide in air, soil, water, and living organisms (Gao et al., 2020; Wang et al., 2020). The thermal and chemical stability of PFOS makes it highly

bioaccumulative and persistent in the environment (Buck et al., 2011). PFOS was the first PFAS to be included in Annex B of the Stockholm Convention on Persistent Organic Pollutants (POPs) (Ahrens and Bundschuh, 2014; Martínez et al., 2019). Relatively high PFOS levels have been detected in wastewaters, sludges, and wastewater treatment plants, along with exposed aquatic organisms, indicating its high bioaccumulation potential (Sant et al., 2021b; Yu et al., 2009; Zareitalabad et al., 2013). Studies investigating PFOS exposure and bioaccumulation in humans revealed that PFOS and related PFAS ranged from 1 to 10 μg/L in blood serum, while concentrations ranged from 10 to 1000 μg/L in highly exposed populations (Armitage et al., 2009; Cao et al., 2018; Inoue et al., 2004). Another study demonstrated that PFOS has a half-life of > 5 years in human serum (Olsen et al., 2007). The detection of PFOS in mammals and aquatic organisms has raised concerns about the potential effects of PFOS exposure (Posner, 2012; Zareitalabad et al., 2013), and toxicological analyses have demonstrated adverse effects of PFOS and related PFAS on growth, development, fertility, immunity, lipid metabolism, the thyroid system, and carcinogenesis (Arrieta-Cortes et al., 2017; Chen et al., 2014; Huang et al., 2010; Martínez et al., 2019; Wang et al., 2023; Xu et al., 2022).

Despite extensive studies on PFOS toxicity, the underlying mechanisms are still poorly understood (Martínez et al., 2019). In vivo and in vitro models face challenges in elucidating the mechanisms by which PFOS exposure affects biological processes and in assessing human health risks (Zeng et al., 2019). Animal experiments have been conducted to inform the evaluation of health risks of PFOS exposure for humans (Krupa et al., 2022; Razak et al., 2023; Sun et al., 2023; Wan et al., 2021; Xu et al., 2022). However, toxicological studies on a wider range of model organisms are required to better understand interspecies variation in response to PFOS exposure (Zeng et al., 2019). Furthermore, the integration of various omics techniques in PFOS studies is required to elucidate the mechanisms of toxicity, since the non-metabolic effects of embryotoxicity and the underlying mode of action of PFOS-induced developmental toxicity are poorly understood.

Xenopus laevis (African clawed frog) is an excellent model organism for the study of the molecular basis of human disease and development because of its genetic similarity with humans (Hellsten et al., 2010; Khokha, 2012). Compared with other model organisms, *X. laevis* has been estimated to share more than 79% of identified human disease genes (Nenni et al., 2019; Tandon et al., 2017). Moreover, the availability of *X. laevis* eggs throughout the year, transparent eggs, and their external development make them an ideal choice for animal model experiments.

Cilia are membrane-bound organelles found in vertebrate cells that play important roles in cell signal transduction and cell fate determination (Nachury and Mick, 2019; Sreekumar and Norris, 2019). Ciliogenesis defects can lead to disruption of cell division and are associated with the malfunctioning of neurons and impaired cardiovascular development (Pala et al., 2018; Wallingford, 2006). Ciliary abnormalities in Kupffer's vesicles resulted in pericardial and yolk sac edema, a bent body axis, and hydrocephalus during embryonic development of the zebrafish (Kramer-Zucker et al., 2005). Furthermore, a previous study reported that exposure to 100 μM PFOS induced an 11% increase in the frequency of ciliary beats by elevating calcium concentrations in the trachea of mice (Matsubara et al., 2007). Another study identified ciliary dysfunction as a probable mode of action for chemical-induced developmental toxicity (Huang et al., 2021). Therefore, we hypothesized that developmental abnormalities induced by PFOS during *X. laevis* embryogenesis could involve changes in cilia.

In the present study, we investigated the embryotoxic potential of PFOS on *X. laevis* using a combination of morphometric and transcriptomic analyses. Ciliary responses to PFOS exposure were studied in developing embryos cell death and adenosine triphosphate (ATP) analyses were performed to contribute to the safety and risk assessment of PFOS as a ubiquitous POP.

2. Materials and methods

2.1. Chemicals and reagents

PFOS ($\geq$ 98% purity) and $CaSO_4 \cdot 2 H_2O$ were purchased from Sigma-Aldrich (St. Louis, MO, USA). NaCl and $NaHCO_3$ were purchased from Amresco (Solon, OH, USA). KCl, $CaCl_2$, and $MgSO_4$ were purchased from Junsei (Tokyo, Japan). The PFOS stock solution (0.1 mM) was prepared in dimethyl sulfoxide and serially diluted with the frog embryo teratogenesis assay *Xenopus* (FETAX) solution to working concentrations. All chemicals and reagents were of analytical grade.

2.2. Maintenance of X. laevis, embryo collection and FETAX

Mature *X. laevis* were obtained from the Korean *Xenopus* Resource Center for Research and maintained in containers under a 12 hr. light: dark cycle at 18 $\pm$ 2 °C. Animals were fed with a semi-synthetic diet thrice weekly. For embryo collection, female *X. laevis* were induced to ovulate by injecting human chorionic gonadotropins in the dorsal lymph sac. The next morning, females were transferred to tanks containing 1 $\times$ high salt solution to lay their eggs. The eggs were collected in 60 mm petri dishes and washed with 0.1 $\times$ modified barth solution (MBS). Male *X. laevis* were placed in benzocaine for 5–15 min and dissected to isolate their testis. The isolated testes were stored in 1 $\times$ MBS at 4 °C. The eggs were fertilized with a sperm suspension solution derived from the isolated testes. After successful fertilization, the jelly coat of the embryos was removed by swirling in 2% L-cysteine and washing with 0.5 $\times$ MBS. Live, healthy embryos were identified and selected for exposure studies following observation under a dissecting microscope.

The embryotoxicity assays were performed in compliance with the standard guide for FETAX with slight modifications (Mouche et al., 2011). Normally cleaved midblastula-stage (Nieuwkoop and Farber's stage 8.5 [NF St. 8.5]) embryos were randomly collected and placed in six-well plates. The embryos were exposed to one of five PFOS concentrations (25, 50, 75, 100, and 125 μM) to calculate the median lethal concentration (LC_{50}) and median effective concentration (EC_{50}) of PFOS for *X. laevis*. The embryos grown in the standard FETAX solution alone served as control embryos. The eggs were obtained from three different females. Assays were performed in triplicate per female containing 25 embryos per assay. The plates containing six treatment groups (each plate contained one replicate for each of the six treatments) were incubated at 23 $\pm$ 2 °C for 96 hr. After 96 hr., all surviving embryos in each treatment group were counted and fixed in MEMFA (4% paraformaldehyde, 0.1 M MOPS [pH 7.4], 1 mM $MgSO_4$, and 2 mM EGTA) to observe malformations under a dissecting microscope (Ismail et al., 2023).

2.3. Alcian blue staining

X. laevis embryos were harvested after 15 days, fixed in MEMFA for 2 hr. at room temperature, and washed with 50% ethanol. The embryos were stained using Alcian blue solution (0.05% Alcian blue 8GX, Sigma-Aldrich, in 10 mM $MgCl_2$/80% ethanol) for 3 days at room temperature. The embryos were washed in 10 mM $MgCl_2$/80% ethanol and bleached in 1% H_2O_2 and 5% formamide/0.5% SSC for 4 hr. The embryos were incubated in 0.1 $\times$ trypsin and washed in methanol (Klymkowsky and Hanken, 1991).

2.4. Ciliogenesis analysis

To investigate the effects of PFOS on ciliogenesis during *X. laevis* embryogenesis, the cilia-driven flow and the number of multiciliated cells (MCCs) were quantified as described below.

a) The cilia-driven flow was quantified using embryos at the tailbud stage (NF St. 23). The embryos were anesthetized using 0.05 $\times$

benzocaine in 0.5 × MBS. Fluorescently labeled polystyrene beads with a diameter of 10 μm (Molecular Probes, Eugene, OR, USA) were dropped on top of the embryos, and the bead flow was recorded by observing the embryos under a fluorescence microscope. The velocity of fluorescent beads was measured using Fluorescent Bead-Measurement Tracker 6.0.

b) Embryos at the tailbud stage (NF St. 23) were stained immunofluorescently according to previously described standards (Dollar et al., 2005), For this, anti-acetylated tubulin (1:1000; Sigma-Aldrich) was used as the primary antibody, followed by incubation with a fluorescein isothiocyanate-conjugated anti-mouse (1:2000; Invitrogen, Carlsbad, CA, USA) as the secondary antibody. Fluorescently labeled embryos were observed under a confocal microscope and the number of MCCs was counted and the appearance of MCCs characterized using GraphPad Prism version 8.0 (GraphPad Software, San Diego, CA, USA).

2.5. Gene expression analysis

Gene expression analysis was performed using whole-mount in situ hybridization (WISH), reverse transcription polymerase chain reaction (RT-PCR), quantitative polymerase chain reaction (qPCR), and transcriptomics, as described below. The organ specific transcripts i.e., *nkx 2–5*, *ldlrap1*, *darmin*, *sox3*, and *pax6* for WISH, RT-PCR, and qPCR were selected because of their association with chemical induced toxicity during *X.laevis* embryonic development (Ismail, 2019; Ismail, 2023).

a) For WISH analysis, *X. laevis* embryos were fixed at the tailbud stage (NF St. 32) in MEMFA overnight at 4 °C and dehydrated before storage in 100% methanol at −20 °C. Antisense digoxigenin (DIG)-labeled probes were synthesized by linearizing the DNA templates using appropriate restriction enzymes. SP6 or T7 RNA polymerases (Ambion, Austin, TX, USA) were used to synthesize the RNA probes containing DIG. DIG-labeled probes were detected using an alkaline phosphatase-labeled anti-DIG antibody (1:1000; Roche, Basel, Switzerland) and nitro blue tetrazolium/5-bromo-4-chloro-3-indolyl phosphate.

b) For PCR analysis, total RNA from *X. laevis* embryos was extracted using an Isol-RNA lysis reagent (5 Prime GmbH, Hilden, Germany). cDNA was synthesized by the PrimeScript™ First-Strand cDNA Synthesis Kit (Takara, Kusatsu, Japan). PCR was performed using customized primers (Table S1) for RT-PCR, the resulting products were separated on 1% agarose gels, and images were captured using a gel analyzer (Wise Capture I-1000; Daihan Scientific, Wonju, South Korea).

c) qPCR was performed using the AccuPower® 2X GreenStar™ qPCR MasterMix (Bioneer, K6253) on a CFX Connect Real-Time PCR Detection System (Bio-Rad). The *odc* gene was used for normalization (Ismail et al., 2023). The primer sequences are given in Table S2.

d) For transcriptomics analysis, the RNA sequencing library was prepared by extracting total RNA from each sample using polyA enrichment according to the manufacturer's instructions (Illumina, San Diego, CA, USA). cDNA sequence reads of *X. laevis* were mapped from the Genome Project Consortium using bwa (version 0.7.15) to estimate mRNA abundance. edgeR (version 3.20.7) was used to analyze differentially expressed genes (DEGs) in R. Genes with a fold change of greater than four and a false discovery rate of < 0.01 in exact tests were considered to show significantly different expression between the PFOS-exposed and control embryos. Overrepresentation of biological processes among the DEGs was identified using Fisher's exact tests on the PANTHER (Protein ANalysis THrough Evolutionary Relationships) platform (released 20171205) with human orthologous genes based on best hits using the basic local alignment search tool program search. Raw data for RNA sequencing are available at the National Center for Biotechnology Information Gene Expression Omnibus database.

2.6. Terminal deoxynucleotidyl transferase-mediated dUTP nick-end labeling (TUNEL) staining and ATP quantification

PFOS-exposed and control *X. laevis* embryos were fixed for 24 hr. in MEMFA at 4 °C and bleached using a bleaching solution (3% H_2O_2, 5% formamide, and 5 × standard saline citrate). After washing with phosphate-buffered saline, the embryos were processed for TUNEL staining, as described previously (Kim et al., 2018).

For ATP quantification, PFOS-exposed and control *X. laevis* embryos were lysed in a lysis buffer (1 M Tris-HCl, 1 M dithiothreitol, glycerol, Triton X-100, and distilled water). The supernatant was collected after centrifugation at 4 °C, and the Bradford assay was performed using a Bio-Rad reagent to measure the amount of protein. The levels of ATP were measured in samples from the PFOS-exposed and control embryos, containing equal amounts of protein, using the ENLITEN® ATP Assay System (Promega, Madison, WI, USA).

2.7. Statistical analysis

Lethality percentages were calculated by dividing the number of dead embryos by the total number of embryos at the beginning of the assay. The percentage of malformations was obtained by dividing the number of malformed larvae by the total number of surviving larvae at the end of the assay. Nonlinear regression analysis was performed to estimate the LC_{50} and EC_{50} values.

Data from WISH and RT-PCR were analyzed using ImageJ software (NIH; http://imagej.nih.gov). Results are presented as the mean ± SE (n = 3 biological replicates, with 25 embryos per replicate for each sample). Differences between groups were analyzed using one-way analysis of variance followed by Dunnett's post-hoc tests for multiple comparisons (Comparison of different concentration of PFOS and control). An unpaired t-test was used to compare the PFOS-exposed and control groups. $P \leq 0.05$ was considered the threshold for significance.

3. Results and Discussion

3.1. PFOS exposure resulted in mortality, growth retardation, and phenotypic abnormalities during embryogenesis

Midblastula-stage *X. laevis* embryos were exposed to a range of PFOS concentrations for 96 hr. to investigate the lethal and teratogenic effects of PFOS. The embryos exhibited dose- and time-dependent toxicity (Fig. S1A). No significant occurrence of lethality or malformations was observed at lower PFOS concentrations, but a higher frequency of lethality and malformations was observed at higher PFOS concentrations in a time-dependent manner resulting in a teratogenic index of 1.62 (Fig. S1B). The toxicity response of *X.laevis* embryos to PFOS was consistent with previous studies conducted in other aquatic species (Huang et al., 2010; Krupa et al., 2022; Razak et al., 2023). The concentrations of PFOS used in this study were higher than the environmentally relevant concentration of PFOS in drinking water, though these higher concentrations may be relevant for industrial wastewater runoff and were selected based on previous studies in the zebrafish (Sant et al., 2021b; Sant et al., 2017b; Zheng et al., 2012b). Studying the effects of higher concentrations of PFOS is relevant since there are diverse routes for PFOS exposure, and PFOS has the potential to bioaccumulate in the environment (Monnot et al., 2023). Moreover, higher concentrations of PFOS are legally used for some purposes (Martínez et al., 2019).

The embryos that survived the 96-hr. exposure experiment were analyzed to determine the morphometric endpoints of skeleton appearance, total body length (TBL), body axis appearance, and gut coiling. Significantly shorter body length was observed in the embryos exposed to PFOS compared with the control embryos (Fig. 1A). The embryos exposed to the highest concentration of PFOS (125 μM) exhibited a significantly shorter body length (5787 μm) than control embryos (8290 μm; Fig. 1B). The embryos exposed to 50 –100 μM PFOS
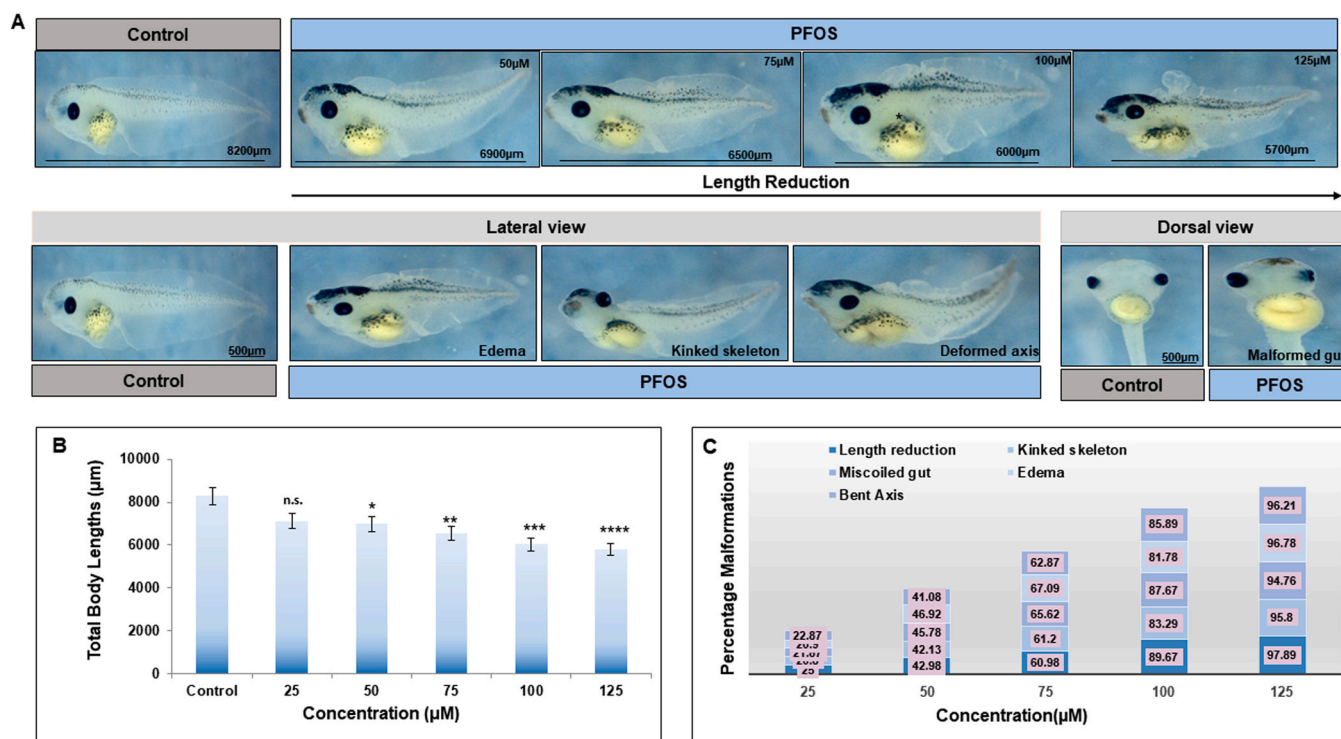
Fig. 1. Phenotypic abnormalities induced by perfluorooctanesulfonate (PFOS) exposure from 0 to 96 hr. post fertilization (hpf). **A.** PFOS exposure from 0 to 96 hpf induced phenotypic abnormalities including length reduction, kinked skeleton, edema, miscoiled gut, and a deformed axis in *X.laevis* embryos compared with control embryos. **B.** PFOS exposure resulted in growth retardation by significantly affecting the total body length (TBL) of developing embryos. The graph shows the dose-dependent response of the TBL of embryos to PFOS exposure (* $P < 0.05$; ** $P < 0.01$; *** $P < 0.001$; ns. = not significant; ANOVA followed by Dunnett's test). **C.** Graphical representation of malformed phenotypes caused by PFOS exposure indicated a concentration-dependent response in exposed embryos. Values are expressed as the mean $\pm$ SE.

showed an average body length of approximately 6000 μm, which was also significantly shorter than the control embryos (Fig. 1B). TBL analysis showed that PFOS affected embryonic growth even at the low PFOS concentrations of 25 and 50 μM. Length reduction is an important toxicological endpoint indicating the toxicity potential of chemicals (Ismail et al., 2019). The length reduction phenomenon observed in developing *X. laevis* embryos is consistent with previous reports of a shorter body length in zebrafish exposed to PFOS (Mahapatra et al., 2023; Sant et al., 2017b; Shi et al., 2008).

The skeletal phenotypic analysis indicated that PFOS exposure resulted in a kinked skeleton and deformed axis in the PFOS-exposed embryos compared with the control embryos in a dose-dependent manner (Fig. 1A and C). Gut-coiling analysis was another endpoint used to assess the toxic effects of PFOS on organ development, showing that exposure to high PFOS concentrations led to fewer coils and a flat gut while the control embryos displayed a properly coiled gut (Fig. 1A and C). The malformed gut of PFOS-exposed embryos exhibited a dose-dependent relationship, clearly indicating the ingestion of PFOS by developing embryos since the embryos exposed to high concentrations of PFOS exhibited an inflated gut while a normally coiled gut was observed in the control embryos. The embryos of *X. laevis* start to open their mouth at NF St. 40 (corresponding to approximately 66 hr. post fertilization [hpf] at 23 °C; Hoke and Ankley, 2005), and the present exposure experiment ended at 96 hpf (NF St. 46). This indicates that embryos could have ingested PFOS for 36–40 hr. of the 96-hr. exposure period. However, analysis of the PFOS-exposed embryos indicated that the intestine was the only organ showing phenotypic abnormalities. In addition to changes in body length and gut coiling, PFOS exposure also resulted in edema in exposed embryos in a dose-dependent manner while the control embryos were morphologically normal (Fig. 1A and C). These morphometric endpoints clearly indicated the teratogenic potential of PFOS during early embryonic life, consistent with previous

studies (Shi et al., 2008; Zheng et al., 2012a) and increasing our knowledge of PFOS-induced developmental defects.

3.2. PFOS exposure resulted in craniofacial defects and a deformed axis at the later stages of embryonic development

X. laevis embryonic growth and morphology were assessed at 15 days post fertilization (dpf) following developmental PFOS exposure from 0 to 96 hpf. The embryos were observed at a later stage of development to investigate whether PFOS-exposed embryos were able to recover normal growth and development following early exposure to PFOS. However, the developmental PFOS exposure induced considerable axis deformations in the exposed embryos compared with the control embryos (Fig. S2A). Approximately 80% of the PFOS-exposed embryos showed axis deformities compared with the control embryos at 15 dpf (Fig. S2B).

In addition to axis deformations, more than 85% of the PFOS-exposed embryos developed smaller heads compared with the control embryos (Fig. S2C and D). Alcian blue cartilage staining was conducted to further observe the anomalies in the cephalic region in PFOS-exposed embryos. The microscopic analysis of the control embryos showed the organization of cranial neural crest cells into branchial arches (Fig. S2C). Moreover, the infrarostral, Meckel's, and palatoquadrate cartilages, constituting the lower and upper jaw, as well as the ceratohyal cartilages and gill basket were all evident in the stained control embryos (Fig. S2C). The most pronounced effects observed after PFOS exposure included small and poorly differentiated infrarostral cartilage as well as changes in the morphology of the Meckel's and palatoquadrate cartilages. Furthermore, the ceratohyal cartilage seemed to be less developed, and the branchial arches exhibited irregular outlines (Fig. S2C). However, no death was observed during the later stages of embryonic development. The morphological abnormalities observed in the PFOS-

exposed embryos support the bioaccumulation potential of PFOS in developing *X. laevis* embryos since it is the most plausible explanation for the accumulation of PFOS in developing embryos in sufficient amounts to incur physiological abnormalities without fatalities (Christou et al., 2021; Dong et al., 2021; Haimbaugh et al., 2022). Another possible explanation for malformations at later stages of embryogenesis in the PFOS-exposed embryos is an irreversible effect of PFOS on the genetic makeup of developing embryos that cannot be reversed even after exposure to PFOS is terminated. However, further studies are required to pinpoint the causes of abnormalities observed at the later stages of embryogenesis in the PFOS-exposed embryos.

3.3. PFOS exposure induced morphological effects in time-specific developmental windows

The PFOS-exposed embryos were observed in three developmental windows, distinct from the observed developmental period of conventional FETAX exposure (NF St. 8.5–46). In the first embryonic developmental window (NF St. 8–20; associated with gastrulation and neurulation), PFOS exposure did not induce any notable phenotypic abnormalities, and the survival rate of exposed embryos was unaffected (Fig. S3A and B). During the second developmental window (NF St. 20–32; early tailbud stage of development and initiation of primary organogenesis), the embryos exhibited sensitivity to PFOS by showing significant lethality and occurrence of malformed phenotypes compared with the control embryos and compared with the conventional FETAX exposure (Fig. S3A and B).

In contrast to the first two developmental windows, considerably higher percentages of malformations and mortality were observed in the PFOS-exposed embryos during the third developmental window (development of primary organs; Fig. S3A and B). More than 80% of the malformed embryos and > 90% of mortality were observed in this

developmental window (Fig. S3A and B). The *X. laevis* embryos were more sensitive to PFOS exposure during the tailbud stage of development. The increased occurrence of lethality and malformations during the second and third developmental windows demonstrated that the absorption of PFOS during these windows was considerably higher than during the first developmental window. The enhanced sensitivity of embryos during the third developmental window could be caused by the increased ingestion ability of embryos during this phase as *X. laevis* embryos start to open the mouth during NF St. 40. However, further investigations are required to elucidate the mechanisms underlying the increased sensitivity of *X. laevis* embryos to PFOS during the second and third developmental windows.

3.4. PFOS exposure perturbed the expression of organ-specific transcripts

Targeted gene expression was observed using organ-specific probes in *X. laevis* embryos during NF St. 32. The homeodomain transcription factor associated with heart development (*nkx2–5*) was upregulated in the PFOS-exposed embryos compared with the control embryos, indicating PFOS toxicity in cardiac development (Fig. 2A and Fig. S4A-C). Transcriptomics revealed that the expression of the heart-associated genes, urotensin 2 (*uts2*) and DNA damage inducible transcript 4 like (*ddit4l*), was perturbed, supporting the findings of the WISH, RT-PCR, and qPCR analyses (Fig. 2B and Fig. S4A-C). The cardiac toxicity observed is consistent with previous studies reporting the cardiotoxic effects of PFOS in adult rats (Wen et al., 2023; Xu et al., 2022). While these studies investigated the PFOS toxic effects during adulthood in rats, our study confirms the effects of PFOS during embryonic development in *X. laevis*.

The liver is the major detoxifying organ, and PFOS exposure has been shown to induce liver toxicity in several species (Guo et al., 2019; Hagenaars et al., 2008; Liang et al., 2019). Our findings are consistent
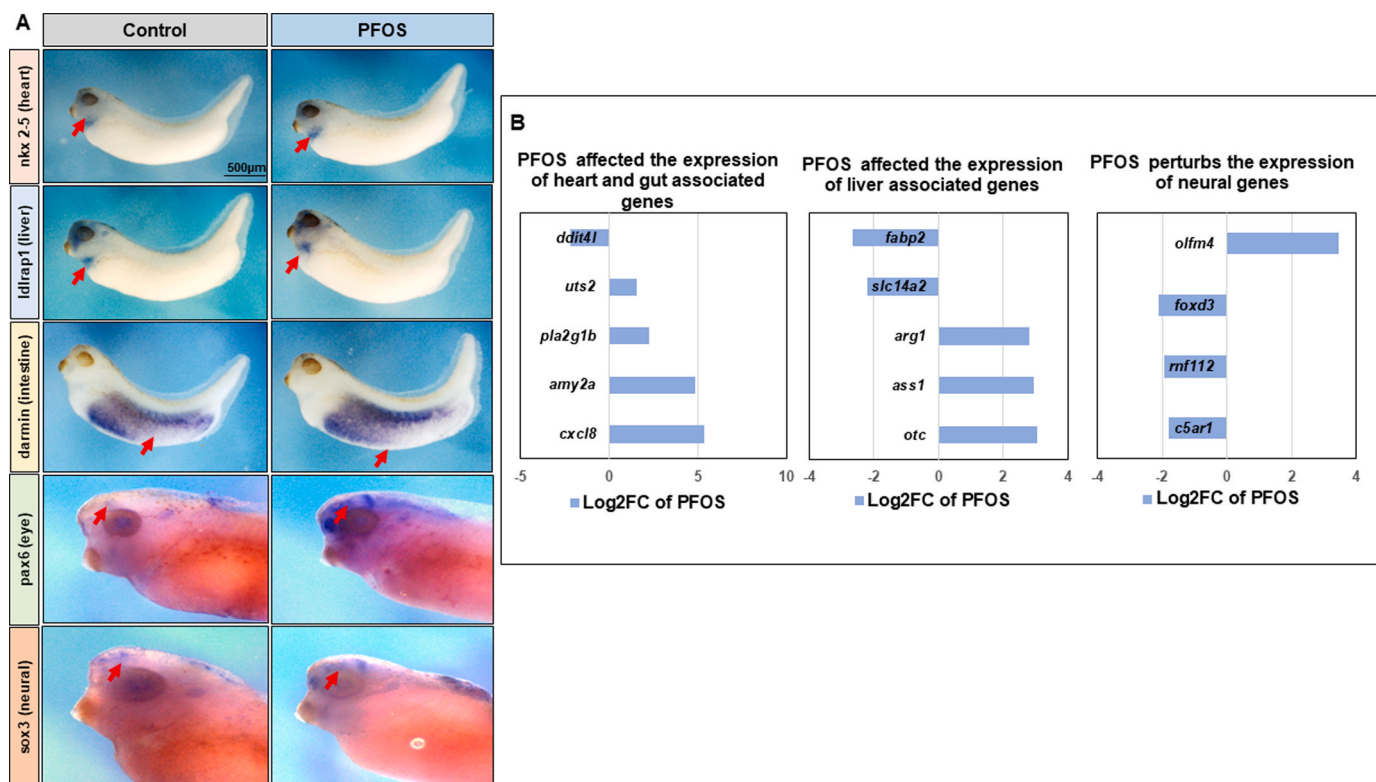

Fig. 2. Perfluorooctanesulfonate (PFOS) exposure perturbed the expression of organ-specific genes in *X. laevis* embryos. **A.** WISH analysis showed that PFOS induced the upregulation of *nkx2–5* (heart-specific), *pax6* (eye and brain-specific), and *sox3* (neural-related) compared with the control embryos, as indicated by red arrows. In contrast, *ldlrap1* (liver-specific) expression was reduced in PFOS-exposed embryos, and *darmin* (intestine-specific) remained unaffected after PFOS exposure, as indicated by red arrows. **B.** Transcriptomics analysis indicated changes in the expression of genes associated with heart, gut, liver, heart, and neural development.

with previous evidence of the liver toxicity effects of PFOS, showing the downregulation of expression of the low-density lipoprotein receptor adaptor protein 1 gene (*ldlrap1*), which has a role in liver development, in the PFOS-exposed embryos (Fig. 2A and Fig. S4). Our transcriptomic analysis also indicated altered expression of genes associated with the urea cycle and liver (ornithine transcarbamylase (*otc*), arginosuccinate synthase 1 (*ass1*), arginase 1 (*arg1*), solute carrier family 14 member 2 (*slc14a2*), and fatty acid binding protein 2 (*fabp2*); Fig. 2D). This altered expression of liver-associated genes is also consistent with the previously reported data from zebrafish embryos (Sant et al., 2021a). The perturbation of liver-associated genes induced by PFOS exposure will help to inform potential PFOS toxicity responses in other species.

We also analyzed the expression of the metallopeptidase gene specific to gut development (*darmin*). The WISH, RT-PCR, and qPCR analyses showed that the expression of *darmin* was not affected by PFOS exposure (Fig. 2 and Fig. S4A-C), but transcriptomics indicated changes in the expression of other genes associated with the digestive system and gut development (C-X-C motif chemokine ligand 8 (*cxcl8*), amylase alpha 2a (*amy2a*), and phospholipase A2 group 1B (*pla2g1b*); Fig. 2D). The contradictory findings of the WISH, PCR, and transcriptomic analyses, in relation to the expression of gut-specific markers, could be because of the different functions of the genes concerned. For example, *darmin* is associated with endoderm development, and expression is restricted to the midgut during the later stages of development (Pera et al., 2003), while the genes showing altered expression are associated with epithelial cells of the intestine and are involved in digestion (Han et al., 2021; Hui, 2019; Neary and Batterham, 2009). Thus, our transcriptomics results demonstrated that PFOS exposure altered the expression of genes associated with gut functions, but it did not alter the expression of genes associated with gut development, and the miscoiling of gut (Fig. 1A) observed in the PFOS-exposed embryos is of an anatomical nature.

The WISH, RT-PCR, and qPCR analyses showed the upregulated expression of the HMG-box transcription factor specific for neural development (*sox3*) and the paired box transcription factor (*pax6*) specific for eye and brain development in PFOS-exposed embryos (Fig. 2A and Fig. S4A-C). Transcriptomic analysis supported the findings of WISH and PCR analyses, indicating the perturbation in the expression of genes associated with neural development (Compliment C5a receptor 1 (*c5ar1*), ring finger protein 112(*rnf112*), forkheadbox D3 (*foxd3*), and olfactomedin 4 (*olfm4*); Fig. 2B). These results provide further support for, and expand our knowledge of, the neurotoxic effects of PFOS as previously shown in zebrafish and mice (Mahapatra et al., 2023; Martínez et al., 2019; Ninomiya et al., 2022).

3.5. PFOS exposure modulated cilia formation and cilia-driven fluid flow during embryogenesis

The important role of cilia during embryonic development is well-understood (Sreekumar and Norris, 2019), and thus it is pertinent to investigate the effects of chemicals on ciliogenesis. The observed malformed axis development during later stages of embryogenesis (Fig. S2A) led us to speculate the involvement of cilia in PFOS-induced embryonic effects. Furthermore, the previously reported ciliary effects of PFOS exposure in the trachea of mice (Matsubara et al., 2007) and developing zebrafish embryos (Huang et al., 2021) led us to investigate the effects of PFOS exposure on ciliogenesis in *X. laevis* embryos. The PFOS-exposed embryos exhibited modulation of MCCs formation (Fig. 3A and B). The number of MCCs was significantly reduced after PFOS exposure in *X. laevis* embryos compared with the control embryos. PFOS exposure affected MCC formation and morphological appearance (Fig. 3).

Along with MCCs, the cilia-generated flow plays an essential role in fluid movements and can act as long-range directional signals (Marshall and Kintner, 2008). The cilia-driven flow is crucial in determining the left–right pattern of the body axis during embryonic development (Marshall and Kintner, 2008). Thus, the effects of PFOS exposure on the cilia-driven flow were investigated using fluorescent microbeads. The
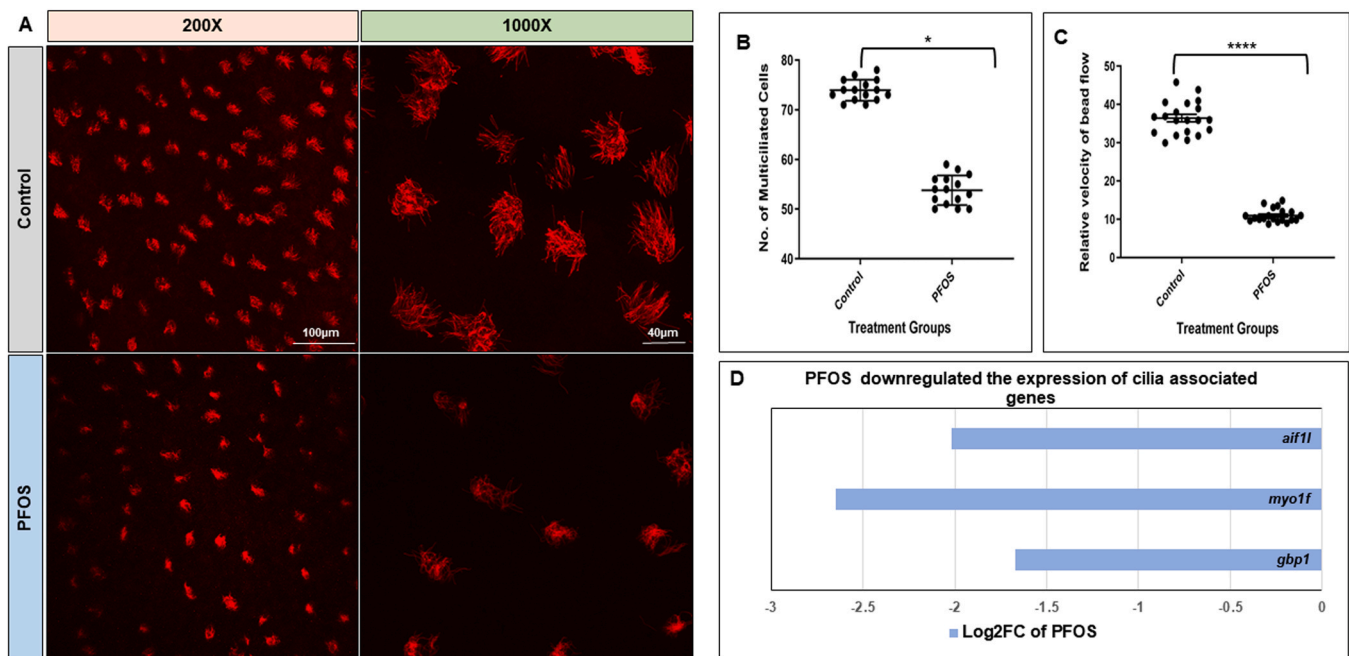
Fig. 3. Effects of perfluorooctanesulfonate (PFOS) exposure on ciliogenesis during *X. laevis* embryogenesis. **A.** PFOS exposure resulted in fewer MCCs compared with the control embryos. Representative figures are shown at 200 × and 1000 × resolution. **B.** Graphical representation of the effects of PFOS exposure on the number of MCCs showing a significant reduction of MCCs compared with the control embryos (* $P < 0.05$; Unpaired t-test / Mann Whitney 's test). **C.** Analysis of fluorescent bead flow driven by cilia revealed that PFOS exposure resulted in a restricted bead flow. The beads tended to flow slowly, without directional motion, compared with the bead flow observed in the control embryos, which showed continuous flow from the anterior end to the posterior end (**** $P < 0.0001$; Unpaired t-test / Mann Whitney 's test). **D.** PFOS exposure downregulated the expression of genes associated with cilia formation.

observed movement of beads was altered in the PFOS-exposed embryos, evidenced by a change in the velocity and a backward bead flow compared with the control embryos (Fig. 3C; Movie S1).

Supplementary material related to this article can be found online at doi:10.1016/j.ecoenv.2023.115820.

Additionally, the transcriptomic analysis indicated a perturbation in the expression of genes associated with actin remodeling and actin accumulation allograft inflammatory factor 1 like (*aif1l*; Yasuda-Yamahara et al., 2018), myosin 1 F (*myo1f*; Barger et al., 2019), and guanylate binding protein 1 (*gbp1*; Ostler et al., 2014); Fig. 3D) in the PFOS-exposed embryos. This suggests that the cilia are the first structure to be affected by PFOS exposure, which subsequently leads to other malformations. However, further studies are required to reveal the mechanisms underlying PFOS toxicity during embryogenesis.

### 3.6. PFOS exposure disrupts biosynthetic and signaling pathways during embryogenesis

High-throughput transcriptomics revealed that 635 of 26,224 expressed genes were differentially expressed between the PFOS-exposed embryos compared with the control embryos (Fig. 4A). Among these 635 DEGs, 345 genes were upregulated in the PFOS-exposed embryos compared with the control embryos, evidenced by a *z*-score greater than 2.5, and 290 transcripts were downregulated, shown by negative *z*-scores (Fig. 4B). Further analysis of the DEGs using PANTHER indicated that PFOS exposure affected various biologically significant pathways, including arginine biosynthesis, plasminogen activating cascade, ornithine degradation, and interleukin signaling (Fig. 4C). Along with these pathways, PFOS exposure downregulated

ATP synthesis, JAK/STAT signaling, and the p53 pathway (Fig. 4D).

The observed PFOS-induced skeletal deformities were also associated with changes in gene expression, as evidenced by altered expression of genes associated with skeletal development (chondroadherin (*chad*) and paired box 1 (*pax1*); Fig. 4E). Transcriptomics also revealed a change in the expression of genes associated with eye development (matrix metallopeptidase 1 (*mmp1*), olfactomedin 4 (*olfm4*), collagen type VIII alpha 2 chain (*col8a2*), and rhodopsin (*rho*); Fig. 4E). These results are in agreement with the skeletal deformities and alterations in eye development observed in zebrafish embryos after PFOS exposure (Hagenaars et al., 2014; Martínez et al., 2019).

Additionally, the transcriptomics analysis supported previously published data (Liu et al., 2018; Sant et al., 2021c; Sant et al., 2017a) indicating that PFOS exposure affected pancreas development since many genes associated with pancreas development and function (carboxyl ester lipase (*cel*), carboxypeptidase B1 (*cpb1*), serine protease 2 (*prss2*), chymotrypsin like elastase 1 (*cela1*); Fig. 4F) were differentially expressed in the PFOS-exposed embryos compared with the control embryos. Thus, these results confirm similar effects of PFOS exposure across species, with limited observed interspecific variation, and increase our knowledge of the effects of PFOS on organisms.

Transcriptomic analysis indicated the upregulation of genes associated with cell death and inhibition of cell proliferation (receptor interacting serine/threonine kinase 3 (*ripk3*), mitogen activated protein kinase kinase 8 (*map3k8*), tumor necrosis factor receptor superfamily member 12a (*tnfrsf12a*), TIMP metallopeptidase inhibitor 1 (*timp1*), TNF alpha induced protein 2 (*tnfaip2*), cholesterol 25-hydroxylase (*ch25h*), stanniocalcin 1 (*stc1*), dual oxidase maturation factor 1 (*duoxa1*), TSR2 ribosome maturation factor (*tsr2*), and acyl CoA synthetase long chain
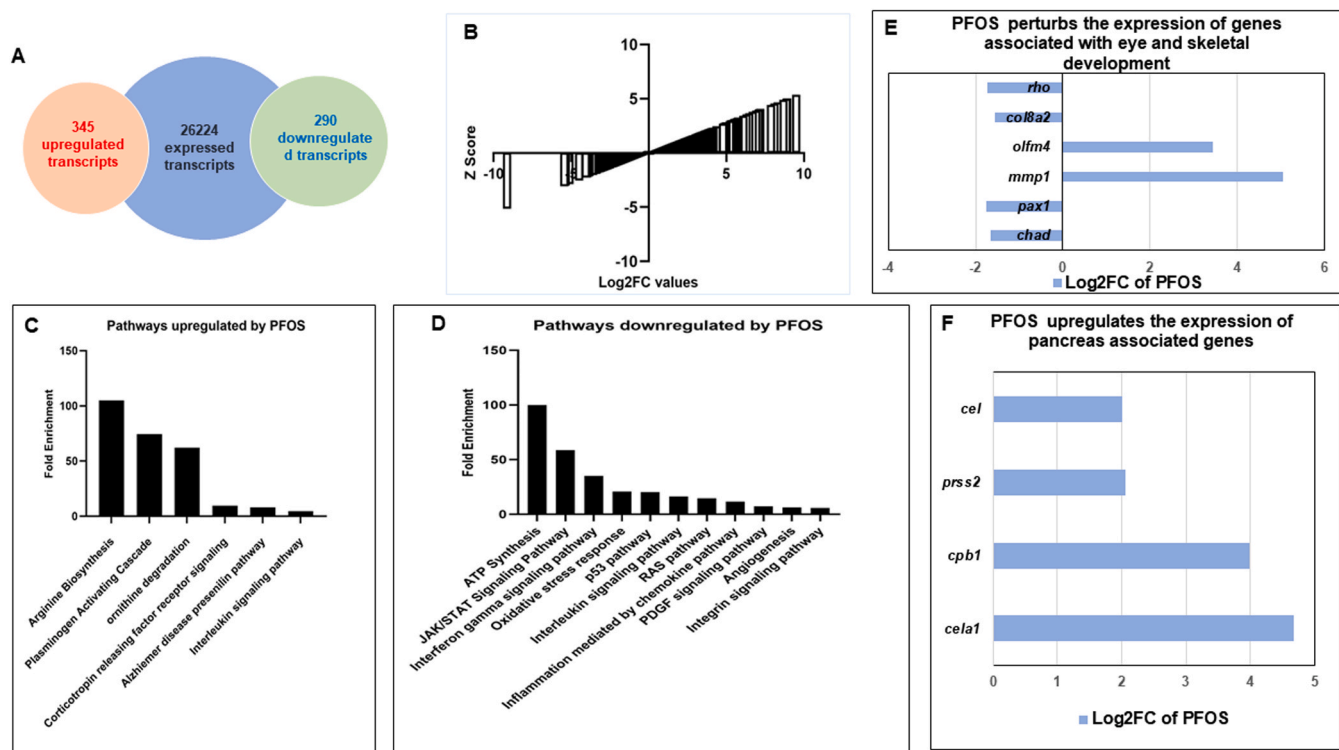
Fig. 4. Perfluorooctanesulfonate (PFOS) exposure resulted in differentially expressed genes (DEGs) in *X. laevis* embryos as analyzed by transcriptomics. **A.** A total of 26,224 transcripts were expressed in PFOS-exposed embryos. PFOS exposure resulted in 635 DEGs in embryos, among which 345 transcripts were upregulated and 290 transcripts were downregulated. **B.** Graphical representation of log two-fold-change values expressed versus *z*-score of the expressed transcripts in PFOS-exposed embryos. Upregulated transcripts showed log two-fold-change values of ≥ 2, whereas downregulated transcripts showed log two-fold-change values of < 2 or − 2. **C.** PFOS exposure resulted in the upregulation of several biosynthesis and signaling pathways, such as arginine biosynthesis, ornithine degradation, interleukin, chemokine signaling, plasminogen activating, and epidermal growth factor receptor signaling. **D.** PFOS resulted in the downregulation of several pathways, including ATP synthesis, oxidative stress response, JAK-STAT signaling, and interferon signaling. **E.** PFOS exposure altered the expression of genes associated with skeleton and eye development as indicated by their log two-fold-change values. **F.** PFOS exposure resulted in the upregulation of genes associated with pancreas development.
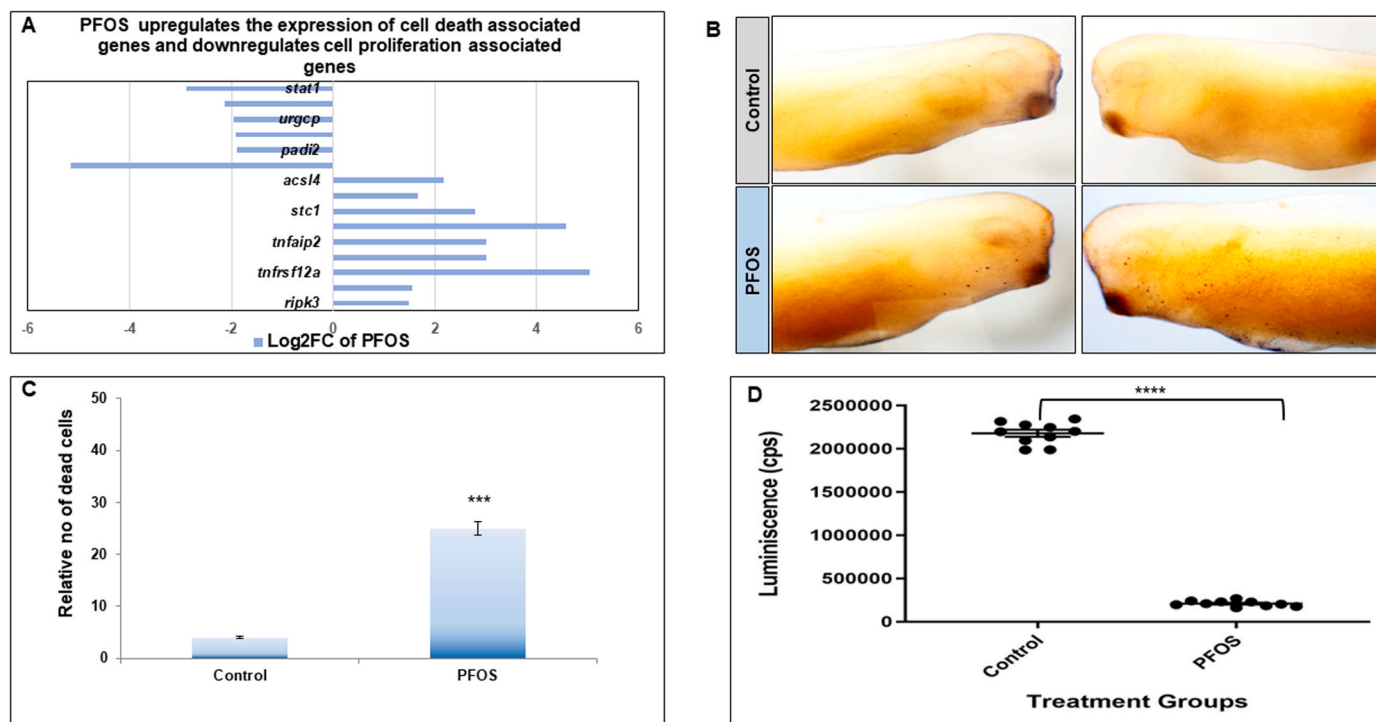
Fig. 5. Perfluorooctanesulfonate (PFOS) exposure increased cell death and reduced relative ATP levels during *Xenopus laevis* embryogenesis. **A.** PFOS treatment resulted in the upregulation of genes associated with cell death and downregulated the genes associated with cell survival and cell proliferation. **B.** PFOS-exposed embryos were processed with a TUNEL assay, and an increased number of TUNEL-positive cells (blue dots) were observed in PFOS-exposed embryos. **C.** Statistical analysis showed a significant number of TUNEL-positive cells in PFOS-exposed embryos compared with control embryos (*** $P < 0.001$; Unpaired t-test / Mann Whitney's Test). **D.** ATP levels were measured in PFOS-exposed embryos and expressed as luminescence (counts per second; cps). The graph shows a significant reduction in luminescence after PFOS exposure compared with the control, indicating a reduction in ATP levels (*** $P < 0.001$; Unpaired t-test / Mann Whitney's Test).

family member 4 (*acsl4*); Fig. 5A) following PFOS exposure. Additionally, genes associated with cell proliferation and survival, including mucin 2 (*muc2*), peptidyl arginine deiminase 2 (*padi2*), apoptosis associated tyrosine kinase (*aatk*), upregulator of cell proliferation (*urgcp*), CD 74 molecule (*cd74*), and signal transducer and activator of transcription 1 (*stat1*), were downregulated in the PFOS-exposed embryos (Fig. 5A). The TUNEL assay results confirmed the findings of transcriptomic analyses since more dead cells were observed in the PFOS-exposed embryos compared with the control embryos (Fig. 5B and C). Most of the dead cells were observed in the eyes, neck, and anterior gut regions of the PFOS-exposed embryos. These results are consistent with the apoptotic effects of PFOS exposure observed in porcine embryos (Leclercq et al., 2022).

The highest fold enrichment observed when comparing the PFOS-exposed and control embryos was linked to the downregulation of the ATP synthesis pathway following PFOS exposure. Thus, we speculated the involvement of bioenergetics in PFOS-induced toxicity, and the findings of the transcriptomics analysis were confirmed by measurements of the relative ATP levels in the PFOS-exposed embryos using an ATP bioluminescence assay. The assay results showed lower ATP levels in the embryos after PFOS exposure compared with the control group (Fig. 5D). Further investigations are required to link PFOS-induced morphometric changes with reduced ATP levels and the effects of PFOS on mitochondrial functions. These findings are consistent with the observed mitochondrial dysfunction in mouse oocytes after PFOS exposure (Jiao et al., 2021).

Collectively, the gene expression profiles, confirmation of cell death by TUNEL assay, and measurement of ATP levels clearly showed that PFOS exposure affected the embryonic development of *X. laevis* by disrupting multiple pathways essential for embryogenesis. Furthermore,

this study increases our knowledge of the effects of PFOS exposure during development, and the findings are consistent with the observed PFOS-induced developmental effects in other model organisms including the zebrafish, mouse, and daphnia.

4. Conclusions

This study suggested a complex mechanism of PFOS toxicity involving ATP synthesis and ciliogenesis, consistent with the previously reported effects of PFOS exposure in other model organisms. Importantly, our findings expand knowledge of PFOS exposure to a different model organism and suggest there is limited variation in PFOS-induced effects between species. This study confirmed that a common trigger could elicit downregulated responses in different model organisms. More detailed studies are required to understand the toxic effects of PFOS exposure in other organisms and recommend minimum acceptable levels for PFOS in the environment to deliver adequate protection of the environment and its inhabitants from the toxic effects of PFOS.

Declaration of competing interest

The authors declare that they have no known competing financial interests or personal relationships that could have appeared to influence the work reported in this paper.

Data availability

Data will be made available on request.

Acknowledgements

Appendix A. Supporting information

Supplementary data associated with this article can be found in the online version at doi:10.1016/j.ecoenv.2023.115820.

References

Ahrens, L., Bundschuh, M., 2014. Fate and effects of poly- and perfluoroalkyl substances in the aquatic environment: a review. Environ. Toxicol. Chem. 33, 1921–1929.

Armitage, J.M., et al., 2009. Modeling the global fate and transport of perfluorooctane sulfonate (PFOS) and precursor compounds in relation to temporal trends in wildlife exposure. Environ. Sci. Technol. 43, 9274–9280.

Arrieta-Cortes, R., et al., 2017. Carcinogenic risk of emerging persistent organic pollutant perfluorooctane sulfonate (PFOS): a proposal of classification. Regul. Toxicol. Pharmacol. 83, 66–80.

Barger, S.R., et al., 2019. Membrane-cytoskeletal crosstalk mediated by myosin-I regulates adhesion turnover during phagocytosis. Nat. Commun. 10, 1249.

Buck, R.C., et al., 2011. Perfluoroalkyl and polyfluoroalkyl substances in the environment: Terminology, classification, and origins. 7, 513–541.

Cao, W., et al., 2018. Perfluoroalkyl substances in umbilical cord serum and gestational and postnatal growth in a Chinese birth cohort. Environ. Int. 116, 197–205.

Chen, J., et al., 2014. Early life perfluorooctanesulphonic acid (PFOS) exposure impairs zebrafish organogenesis. Aquat. Toxicol. 150, 124–132.

Christou, M., et al., 2021. Developmental exposure to a POPs mixture or PFOS increased body weight and reduced swimming ability but had no effect on reproduction or behavior in zebrafish adults. Aquat. Toxicol. 237, 105882.

Dollar, G.L., et al., 2005. Regulation of Lethal giant larvae by Dishevelled. 437, 1376–1380.

Dong, G., et al., 2021. Exploration of the developmental toxicity of TCS and PFOS to zebrafish embryos by whole-genome gene expression analyses. Environ. Sci. Pollut. Res Int 28, 56032–56042.

Gao, Y., et al., 2020. Perfluorooctane sulfonate enhances mRNA expression of PPARγ and ap2 in human mesenchymal stem cells monitored by long-retained intracellular nanosensor. 263, 114571.

Guo, J., et al., 2019. The PFOS disturbed immunomodulatory functions via nuclear Factor-κB signaling in liver of zebrafish (Danio rerio). Fish. Shellfish Immunol. 91, 87–98.

Hagenaars, A., et al., 2008. Toxicity evaluation of perfluorooctane sulfonate (PFOS) in the liver of common carp (Cyprinus carpio). Aquat. Toxicol. 88, 155–163.

Hagenaars, A., et al., 2014. PFOS affects posterior swim bladder chamber inflation and swimming performance of zebrafish larvae. Aquat. Toxicol. 157, 225–235.

Haimbaugh, A., et al., 2022. Multi- and transgenerational effects of developmental exposure to environmental levels of PFAS and PFAS mixture in Zebrafish (Danio rerio). Toxics 10.

Han, Z.J., et al., 2021. Roles of the CXCL8-CXCR1/2 axis in the tumor microenvironment and immunotherapy. Molecules 27.

Hellsten, U., et al., 2010. The genome of the Western clawed frog Xenopus tropicalis. 328, 633–636.

Hoke, R.A., Ankley, G.T., 2005. Application of frog embryo teratogenesis assay-Xenopus to ecological risk assessment. Environ. Toxicol. Chem. 24, 2677–2690.

Huang, H., et al., 2010. Toxicity, uptake kinetics and behavior assessment in zebrafish embryos following exposure to perfluorooctanesulphonicacid (PFOS). Aquat. Toxicol. 98, 139–147.

Huang, J., et al., 2021. Developmental toxicity of the novel PFOS alternative OBS in developing zebrafish: an emphasis on cilia disruption. J. Hazard. Mater. 409, 124491.

Hui, D.Y., 2019. Group 1B phospholipase A(2) in metabolic and inflammatory disease modulation. Biochimica et biophysica acta. Mol. Cell Biol. Lipids 1864, 784–788.

Inoue, K., et al., 2004. Perfluorooctane sulfonate (PFOS) and related perfluorinated compounds in human maternal and cord blood samples: assessment of PFOS exposure in a susceptible population during pregnancy. Environ. Health Perspect. 112, 1204–1207.

Ismail, T., et al., 2019. Comparative analysis of the developmental toxicity in Xenopus laevis and Danio rerio induced by Al2O3 nanoparticle exposure. 38, 2672–2681.

Ismail, T., et al., 2023. PCNB exposure during early embryogenic development induces developmental delay and teratogenicity by altering the gene expression in Xenopus laevis. Environ. Toxicol. 38, 216–224.

Jiao, X., et al., 2021. Perfluorononanoic acid impedes mouse oocyte maturation by inducing mitochondrial dysfunction and oxidative stress. Reprod. Toxicol. 104, 58–67.

Khokha, M.K.J., 2012. Xenopus white papers and resources: folding functional genomics and genetics into the frog. 50, 133–142.

Kim, Y., et al., 2018. Physiological effects of KDM5C on neural crest migration and eye formation during vertebrate development. 11, 1–17.

Klymkowsky, M.W., Hanken, J., 1991. Whole-mount staining of Xenopus and other vertebrates. Methods Cell Biol. 36, 419–441.

Kramer-Zucker, A.G., et al., 2005. Cilia-driven fluid flow in the zebrafish pronephros, brain and Kupffer's vesicle is required for normal organogenesis. Development 132, 1907–1921.

Krupa, P.M., et al., 2022. Chronic aquatic toxicity of perfluorooctane sulfonic acid (PFOS) to Ceriodaphnia dubia, Chironomus dilutus, Danio rerio, and Hyalella azteca. Ecotoxicol. Environ. Saf. 241, 113838.

Leclercq, A., et al., 2022. Occurrence of late-apoptotic symptoms in porcine preimplantation embryos upon exposure of oocytes to perfluoroalkyl substances (PFASs) under in vitro meiotic maturation. PLoS One 17, e0279551.

Liang, X., et al., 2019. Effect of prenatal PFOS exposure on liver cell function in neonatal mice. Environ. Sci. Pollut. Res Int 26, 18240–18246.

Liu, S., et al., 2018. PFOA and PFOS disrupt the generation of human pancreatic progenitor cells. Environ. Sci. Technol. Lett. 5, 237–242.

Ma, T., et al., 2023. Toxicity of per- and polyfluoroalkyl substances to aquatic vertebrates. 11.

Mahapatra, A., et al., 2023. Unraveling the mechanisms of perfluorooctanesulfonic acid-induced dopaminergic neurotoxicity and microglial activation in developing zebrafish. Sci. Total Environ. 887, 164030.

Marshall, W.F., Kintner, C., 2008. Cilia orientation and the fluid mechanics of development. Curr. Opin. Cell Biol. 20, 48–52.

Martínez, R., et al., 2019. Unravelling the mechanisms of PFOS toxicity by combining morphological and transcriptomic analyses in zebrafish embryos. Sci. Total Environ. 674, 462–471.

Matsubara, E., et al., 2007. Effects of perfluorooctane sulfonate on tracheal ciliary beating frequency in mice. Toxicology 236, 190–198.

Monnot, A.D., et al., 2023. Can oral toxicity data for PFAS inform on toxicity via inhalation? Risk Anal. 43, 1533–1538.

Mouche, I., et al., 2011. FETAX assay for evaluation of developmental toxicity. Methods Mol. Biol. 691, 257–269.

Nachury, M.V., Mick, D.U., 2019. Establishing and regulating the composition of cilia for signal transduction. Nat. Rev. Mol. Cell Biol. 20, 389–405.

Neary, M.T., Batterham, R.L., 2009. Gut hormones: Implications for the treatment of obesity. Pharmacol. Ther. 124, 44–56.

Nenni, M.J., et al., 2019. Xenbase: facilitating the use of Xenopus to model human disease. Front Physiol. 10, 154.

Ninomiya, A., et al., 2022. The neurotoxic effect of lactational PFOS exposure on cerebellar functional development in male mice. Food Chem. Toxicol. 159, 112751.

Olsen, G.W., et al., 2007. Half-life of serum elimination of perfluorooctanesulfonate, perfluorohexanesulfonate, and perfluorooctanoate in retired fluorochemical production workers, 115, 1298–1305.

Ostler, N., et al., 2014. Gamma interferon-induced guanylate binding protein 1 is a novel actin cytoskeleton remodeling factor. Mol. Cell Biol. 34, 196–209.

Pala, R., et al., 2018. The roles of primary cilia in cardiovascular diseases. Cells 7.

Pera, E.M., et al., 2003. Darmin is a novel secreted protein expressed during endoderm development in Xenopus. Gene Expr. Patterns 3, 147–152.

Posner, S., 2012. Perfluorinated Compounds: Occurrence and Uses in Products. Polyfluorinated Chemicals and Transformation Products. Springer, pp. 25–39.

Razak, M.R., et al., 2023. Acute toxicity and risk assessment of perfluorooctanoic acid (PFOA) and perfluorooctanesulfonate (PFOS) in tropical cladocerans Moina micrura. Chemosphere 313, 137377.

Sant, K.E., et al., 2017a. Embryonic exposures to perfluorooctanesulfonic acid (PFOS) disrupt pancreatic organogenesis in the zebrafish, Danio rerio. Environ. Pollut. (Barking, Essex: 1987) 220, 807–817.

Sant, K.E., et al., 2017b. Embryonic exposures to perfluorooctanesulfonic acid (PFOS) disrupt pancreatic organogenesis in the zebrafish. Danio rerio. 220, 807–817.

Sant, K.E., et al., 2021a. Developmental exposures to perfluorooctanesulfonic acid (PFOS) impact embryonic nutrition, pancreatic morphology, and adiposity in the zebrafish, Danio rerio. Environ. Pollut. (Barking, Essex: 1987) 275, 116644-116644.

Sant, K.E., et al., 2021b. Developmental exposures to perfluorooctanesulfonic acid (PFOS) impact embryonic nutrition, pancreatic morphology, and adiposity in the zebrafish, Danio rerio. Environ. Pollut. 275, 116644.

Sant, K.E., et al., 2021c. Developmental exposures to perfluorooctanesulfonic acid (PFOS) impact embryonic nutrition, pancreatic morphology, and adiposity in the zebrafish, Danio rerio. Environ. Pollut. 275, 116644.

Shi, X., et al., 2008. Developmental toxicity and alteration of gene expression in zebrafish embryos exposed to PFOS. Toxicol. Appl. Pharmacol. 230, 23–32.

Sreekumar, V., Norris, D.P., 2019. Cilia and development. Curr. Opin. Genet. Dev. 56, 15–21.

Sun, J., et al., 2023. Multiple toxicity evaluations of perfluorooctane sulfonate on intact planarian Dugesia japonica. Environ. Sci. Pollut. Res Int 30, 60932–60945.

Tandon, P., et al., 2017. Expanding the genetic toolkit in Xenopus: Approaches and opportunities for human disease modeling. 426, 325–335.

Wallingford, J.B., 2006. Planar cell polarity, ciliogenesis and neural tube defects. Hum. Mol. Genet. 15, R227–R234.

Wan, H.T., et al., 2021. Characterization of PFOS toxicity on in-vivo and ex-vivo mouse pancreatic islets. Environ. Pollut. 289, 117857.

Wang, G., et al., 2020. Intestinal environmental disorders associate with the tissue damages induced by perfluorooctane sulfonate exposure, 197, 110590.

Wang, W., et al., 2023. The effects of perfluoroalkyl and polyfluoroalkyl substances on female fertility: a systematic review and meta-analysis. Environ. Res 216, 114718.

Wen, Z.J., et al., 2023. A review of cardiovascular effects and underlying mechanisms of legacy and emerging per- and polyfluoroalkyl substances (PFAS). Arch. Toxicol. 97, 1195–1245.

Xu, D., et al., 2022. Perfluorooctane sulfonate induces heart toxicity involving cardiac apoptosis and inflammation in rats. Exp. Ther. Med 23, 14.

Yasuda-Yamahara, M., et al., 2018. AIF1L regulates actomyosin contractility and filopodial extensions in human podocytes. PLOS ONE 13, e0200487.

Yu, J., et al., 2009. Perfluorooctane sulfonate (PFOS) and perfluorooctanoic acid (PFOA) in sewage treatment plants. Water Res. 43, 2399–2408.

Zareitalabad, P., et al., 2013. Perfluorooctanoic acid (PFOA) and perfluorooctanesulfonic acid (PFOS) in surface waters, sediments, soils and wastewater–a review on concentrations and distribution coefficients. Chemosphere 91, 725–732.

Zeng, Z., et al., 2019. Assessing the human health risks of perfluorooctane sulfonate by in vivo and in vitro studies. Environ. Int. 126, 598–610.

Zheng, X.-M., et al., 2012a. Effects of perfluorinated compounds on development of zebrafish embryos. Environ. Sci. Pollut. Res. 19, 2498–2505.

Zheng, X.-M., et al., 2012b. Effects of perfluorinated compounds on development of zebrafish embryos, 19, 2498–2505.